ROCKY MOUNTAIN
JOURNAL OF MATHEMATICS
Volume 8, Numbers 1 and 2,
Winter and Spring 1978

# APPLICATIONS OF THE INVERSE SCATTERING TRANSFORM II: THE THREE-WAVE RESONANT INTERACTION*

D. J. KAUP

ABSTRACT. The techniques in the preceding paper are applied to the three-wave resonant interaction. With the aid of computer simulations and these techniques, we can almost completely describe how this system evolves in terms of the nonlinear concepts of IST. As in the McCall-Hahn area theorem, the final areas are found to be functions of only the initial areas. Also, the final radiation densities are functions of only the initial radiation densities, and the final soliton spectrum is dependent only on the initial soliton spectrum. We discuss all three subcases and give examples of each.

1. **Introduction.** As we have already seen in the case of self-induced transparency [1], three pieces of direct scattering data determine a relatively large amount of information about the system. When the envelope of the field is real, a reflection coefficient at $\zeta = 0$ determines the area of the envelope. The energy of the envelope can be obtained from a reflection coefficient for real $\zeta$. The bound state eigenvalues and their normalization coefficients determine the final soliton configuration.

As we turn to the three-wave resonant interaction (3WRI), we shall find that a relatively large amount of information can be obtained from the same three pieces of data. Furthermore, when this information is coupled with computer simulations of 3WRI [2], we obtain a virtually complete picture of this interaction. We should emphasize that not only will the simulations verify the theoretical predictions, but they will also give results that theory cannot obtain, as well as suggest additional theoretical interpretations.

In a unitless form, the equations for the envelopes in the 3WRI are given by

$$Q_{1t} + c_1 Q_{1x} = \gamma_1 Q_2^* Q_3^*, \tag{1a}$$

$$Q_{2t} + c_2 Q_{2x} = \gamma_2 Q_1^* Q_3^*, \tag{2a}$$

$$Q_{3t} + c_3 Q_{3x} = \gamma_3 Q_1^* Q_2^*, \tag{3a}$$

where $Q_1(x, t)$ are the envelopes, $c_i$ are the corresponding group velocities, which are ordered according to

*Research supported in part by the National Science Foundation.

(2) $$c_1 < c_2 < c_3,$$

and

(3) $$\gamma_1 = \operatorname{sgn}(E_i \times \omega_i).$$

In (3) $E_i$ is the energy of the $i$th envelope and $\omega_i$ is the corresponding resonant frequency; their relative signs are determined from

(4) $$\omega_1 + \omega_2 + \omega_3 = 0.$$

*The general inverse scattering solution of* (1) was first suggested by Zakharov and Manakov [3], the complete solution of which has been given by them [4] and Kaup [5]. Here, we shall not need the complete solution, and shall immediately proceed to simplify the problem.

Of course, the first step in the inverse scattering method is to find an appropriate linear eigenvalue problem, which will then transform the nonlinear equation into an explicitly integrable form. For the 3WRI (1), the appropriate linear system is the Zakharov-Manakov (ZM) eigenvalue problem [3], [4], [5]

(5a) $$-iv_{1x} + V_{12}v_2 + V_{13}v_3 = -c_1\zeta v_1,$$

(5b) $$-iv_{2x} + V_{21}v_1 + V_{23}v_3 = -c_2\zeta v_2,$$

(5c) $$-iv_{3x} + V_{31}v_1 + V_{32}v_2 = -c_3\zeta v_3,$$

where in (5), the potentials, $V_{ij}$, are related to the envelopes by

(6a) $$V_{23} = \frac{-iQ_1}{\sqrt{(c_2 - c_1)(c_3 - c_1)}}, \quad V_{32} = -\gamma_3\gamma_2 V_{23}{}^*,$$

(6b) $$V_{31} = \frac{-iQ_2}{\sqrt{(c_2 - c_1)(c_3 - c_2)}}; \quad V_{13} = +\gamma_1\gamma_3 V_{31}{}^*,$$

(6c) $$V_{12} = \frac{-iQ_3}{\sqrt{(c_3 - c_1)(c_3 - c_2)}}; \quad V_{21} = -\gamma_1\gamma_2 V_{12}{}^*$$

A key step [4], [5] in the analysis of the ZM eigenvalue problem is the realization that, when the envelopes $Q_i$ do not overlap, the ZM structure reduces to three Zakharov-Shabat (ZS) eigenvalues problems, each of the form [6]

(7a) $$u_{1x} + i\lambda u_1 = qu_2,$$

(7b) $$u_{2x} - i\lambda u_2 = ru_2.$$

For each envelope $Q_i$, the corresponding values for $r$, $q$, and $\lambda$ are related to $Q_i$, $\gamma_i$, $c_i$ and $\zeta$ by

$$q^{(1)} = \frac{-\gamma_2\gamma_3 Q_1^{\,*}}{\sqrt{(c_2 - c_1)(c_3 - c_1)}}, \quad r^{(1)} = +\gamma_2\gamma_3 q^{(1)*},$$

(8a)

$$\lambda^{(1)} = \frac{\zeta}{2}(c_3 - c_2),$$

$$q^{(2)} = \frac{-Q_2}{\sqrt{(c_2 - c_1)(c_3 - c_2)}}, \quad r^{(2)} = -\gamma_1\gamma_3 q^{(2)*},$$

(8b)

$$\lambda^{(2)} = \frac{\zeta}{2}(c_3 - c_1),$$

$$q^{(3)} = \frac{-\gamma_1\gamma_2 Q_3^{\,*}}{\sqrt{(c_3 - c_1)(c_3 - c_2)}}; \quad r^{(3)} = +\gamma_1\gamma_2 q^{(3)*},$$

(8c)

$$\lambda^{(3)} = \frac{\zeta}{2}(c_2 - c_1).$$

Upon this reduction, each envelope is then described by a set of ZS scattering data, consisting of ZS solitons and radiation. Thus, when we use the terms "soliton" and "radiation," we shall be using them in this context. Namely, each envelope, via (7) and (8), is decomposed into ZS solitons and radiation.

Of course, from these three sets of ZS scattering data, we can construct [4], [5] the scattering data of the original ZM problem. But, the manner of construction will depend on the ordering of the envelopes. In Figure 1a, we indicate the ordering of the initial state, where $Q_3$ is to the left of $Q_2$, which is to the left of $Q_1$. In Fig. 1b, we indicate the final state (assuming that the envelopes will separate), and we see that the ordering is now reversed.

Let us start with a configuration as in Figure 1a. From (7) and (8) at $t = 0$, we can decompose each envelope into a set of ZS scattering data, from which we can then construct the ZM scattering data. Knowing how the ZM scattering data evolves in time [4], [5], we can pass through the region of time during which the envelopes are interacting, into the final state at some time $t_f$. (During the interaction, the envelopes are overlapping, in which case the ZM problem cannot be reduced to 3 ZS problems. Thus in this interaction region, strictly speaking, we cannot consider the envelopes to be composed of ZS solitons and radiation.) At $t_f$, we have the configuration as indicated in Figure 1b, assuming that the envelopes separate. Now, we can reverse the above procedure. Given the ZM scattering data, we can systematically decompose it [4], [5] into the 3 sets of ZS scattering data.

Schematically, if we let S be the scattering data of (5), $S^{(i)}$ be the

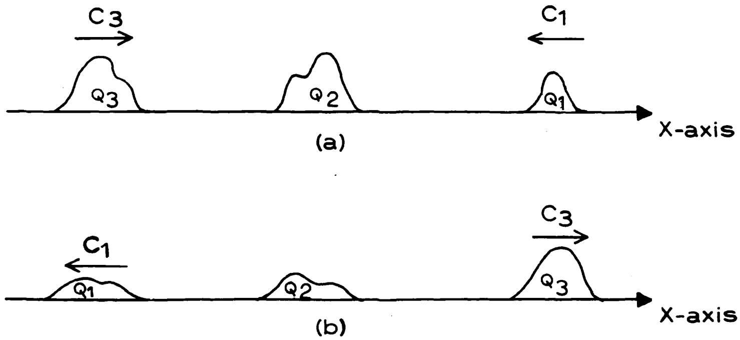


Figure 1. The spacial ordering of the (a) initial and (b) final envelopes.

three sets of Zakharov-Shabat scattering data, one for each envelope, we have that the method of solution is

$$
\begin{aligned}
Q_1, Q_2, Q_3(t=0) &\rightarrow S^{(1)}, S^{(2)}, S^{(3)}(t=0) \\
&\rightarrow S(t=0) \rightarrow S(t_f) \\
&\rightarrow S^{(1)}, S^{(2)}, S^{(3)}(t_f) \\
&\rightarrow Q_1, Q_2, Q_3(t_f),
\end{aligned} \tag{9}
$$

where $t_f$ is any time after separation occurs.

Now, if we define the ZS $a(\lambda)$, $b(\lambda)$, $\bar{a}(\lambda)$, and $\bar{b}(\lambda)$ in the usual manner [7], step 2 to step 5 in (9) reduces [5] to

$$\frac{b_f^{(3)}}{a_f^{(3)}} = \frac{a_0^{(1)}b_0^{(3)} + a_0^{(3)}b_0^{(2)}\bar{b}_0^{(1)}}{a_0^{(2)}a_0^{(3)}}\, e^{-2i\lambda^{(3)}c_3t_f}, \tag{10a}$$

$$\frac{b_f^{(2)}}{a_f^{(2)}} = \frac{a_f^{(3)}}{a_0^{((2)}a_0^{(3)}}\left[a_0^{(3)}b_0^{(2)}\bar{a}_0^{(1)} - b_0^{(1)}b_0^{(3)}\right] \times e^{-2i\lambda^{(2)}c_2t_f}, \tag{10b}$$

$$\frac{b_f^{(1)}}{a_f^{(1)}} = \frac{a_f^{(2)}}{a_0^{(1)}a_0^{(2)}}\left[\bar{a}_f^{(3)}a_0^{(2)}b_0^{(1)} + \bar{b}_f^{(3)}b_0^{(2)}\right] \times e^{-2i\lambda^{(1)}c_1t_f}, \tag{10c}$$

where the arguments of the $a$'s and $b$'s are understood to be the corresponding $\lambda^{(n)}$'s, all of which are related to $\zeta$ via (8).

From (10), since we can determine the scattering data of the final envelopes, we could clearly reconstruct the final envelopes from the ZS inverse scattering equations [6], [7], but as in the previous paper [1], this we shall not need to do. Rather, directly from, and only with (10), we shall be able to obtain a wealth of information. For example, consider the phenomenon of soliton exchange [5]. For simplicity, we take the initial envelopes to be on compact support, so that the initial ZS scattering data will be entire functions of $\zeta$. Since the solitons are determined by the bound state eigenvalues, which are the zeros of $a$ for $\zeta$ in the upper half plane, from (10a) it follows that wherever $a_0^{(2)}$ and $a_0^{(3)}$ have zeros in the upper half plane, $a_f^{(3)}$ will also. Then (10b) shows that $a_f^{(2)}$ can have no zeros in the upper half plane, and (10c) shows that wherever $a_0^{(1)}$ and $a_0^{(2)}$ has a zero, $a_f^{(1)}$ will have a zero. Thus, we can immediately conclude that if $Q_1$, $Q_2$, and $Q_3$ have $N_1$, $N_2$, and $N_3$ solitons respectively initially, then in the final envelopes $Q_1$, $Q_2$, and $Q_3$ will have $N_1 + N_2$, 0, and $N_2 + N_3$ solitons respectively. This is pictorially represented in Figure 2. Furthermore, from the relations between the $\lambda^{(n)}$'s in (10), we know the eigenvalues for the final solitons, and by evaluating the residues of $b_f/a_f$ at these eigenvalues, we can also determine the normalization constants which fix the positions of the solitons.

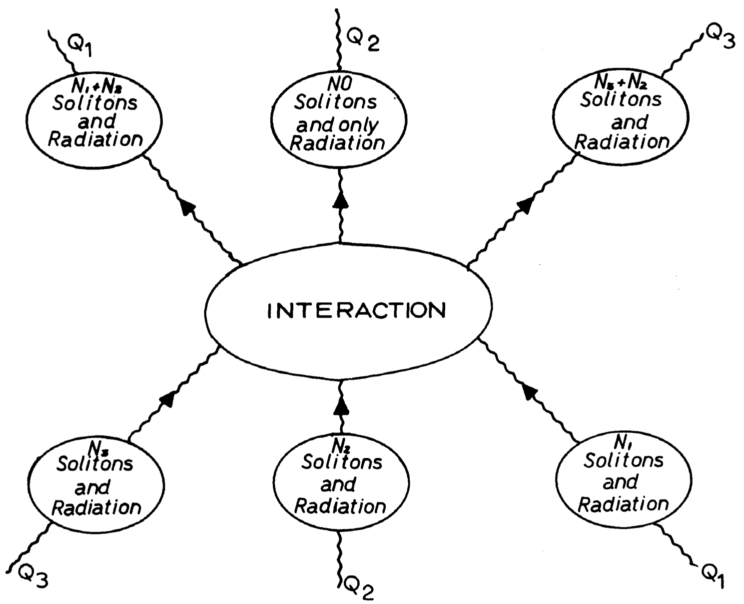


Figure 2. A graphic explanation of how the solitons in the initial envelopes are exchanged to form the final envelopes.

Thus, we can completely determine the soliton configuration in the final envelopes.

Next, consider the area theorem. As we have already seen [1], when the envelope $q$ is real, we have for $r = -q^*$

(11a) $$b(\zeta = 0) = -\sin A,$$

(11b) $$a(\zeta = 0) = +\cos A,$$

where now

(12) $$A \equiv \int_{-\infty}^{\infty} q\, dx.$$

Similarly, if $r = +q^*$, we have

(13a) $$b(\zeta = 0) = +\sinh A,$$

(13b) $$a(\zeta = 0) = +\cosh A,$$

with $A$ still defined as in (12). From (10) and (11–13), we then can obtain the areas of the final envelopes in terms of the areas of the initial envelopes. Note that this gives the final areas as functions *only* of the initial areas, *independent of the structure of the initial envelopes.*

Finally, we can also discuss how the radiation is exchanged between the envelopes. To plasma physicists, this quantity is known as "action", and we define it as

(14) $$N = \int_{-\infty}^{\infty} q^* q\, dx.$$

As in SIT, this can also be given in terms of the scattering data, and is given by [8]

(15) $$N = N_r + N_s,$$

where

(16) $$N_s = 2i \sum_{j=1}^{N} (\lambda_j^* - \lambda_j),$$

(17) $$N_r = \frac{1}{\pi} \int_{-\infty}^{\infty} d\lambda \ln[1 + \Gamma(\lambda)],$$

(in the nonlinear Schrödinger equation, $N_r$ is the total number of radiation "particles" [9]) and we shall call $\Gamma$ the "radiation density". Again, we note that from (10), we can determine $\Gamma(\lambda)$ for each of the final envelopes, upon knowing the initial $\Gamma$'s. Thus by doing the integral in

(17), we can determine the total radiation in each of the final envelopes where when $r = -q^*$,

$$\Gamma(\lambda) \equiv \left| \frac{b}{a}(\lambda) \right|^2, \tag{18a}$$

and when $r = +q^*$,

$$\Gamma(\lambda) \equiv |b(\lambda)|^2. \tag{18b}$$

With $\Gamma$ defined in this manner, we have that whenever

$$\int_{-\infty}^{\infty} |q| < \infty, \tag{19}$$

that [8]

$$0 \leqq \Gamma(\lambda) < \infty. \tag{20}$$

In (17), we shall call $N_r$ the "total" radiation.

2. **The Explosive Case.** Let's now look at some examples from computer simulations. First, for the explosive instability, we typically have the middle envelope, $Q_2$, as being a negative energy wave in a plasma, which also has the highest frequency, so that $|\omega_2| = |\omega_1| + |\omega_3|$. Thus our $\gamma_i$'s in (1) can all be taken to be equal to $-1$, which by (8) gives

$$r^{(1)} = +q^{(1)*}, \tag{21$a$}$$

$$r^{(2)} = -q^{(2)*}, \tag{21b}$$

$$r^{(3)} = +q^{(3)*}. \tag{21c}$$

Now, if (19) is satisfied, it follows [7] that when $r = +q^*$, the eigenvalue problem (7) is self-adjoint, and thus no solitons will exist. (If $r = -q^*$ and (19) is satisfied, no restrictions are placed on solitons.) Consider what happens when $q^{(2)}$ does have one soliton initially. By the soliton exchange in Figure 2, both $q^{(1)}$ and $q^{(3)}$ must then have one soliton in their final envelopes. But by the above, since $r = +q^*$ for these envelopes, they are forbidden from having solitons, if (19) is to remain true. Thus, we have a contradiction, and to see what happens in this case, we look at computer simulations. In Figure 3a, we have the initial profiles, for $A_2 = 2.4131 > \pi/2$ and where $Q_1$ is a perturbation for starting the interaction. (This area, $A$, is one-half of the area, $\theta$, in SIT. Thus here, the critical area for producting $N$ solitons is $(N - 1/2)\pi$.) In Figure 3b and 3c, we see the solution at later times. Note the change in the vertical scales. Clearly, the solution is becoming singular, and this occurs in a finite time, whence the name "explosive instability."

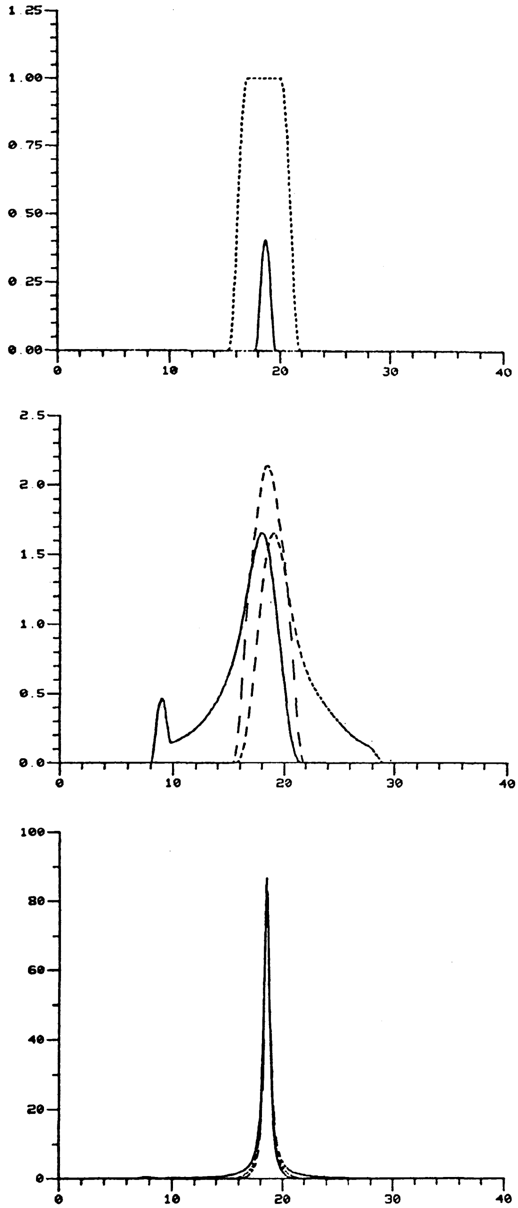


Figure 3. The explosive instability when the area of the middle envelope, $A_2$, is $2.4131 > \pi/2$. In Figure 3a we have the initial configuration with a small amount of $Q_1$ (solid line) to start the interaction. In Figure 3b, runaway growth has started, and in Figure 3c, a spike is forming. Note the change in vertical scales.

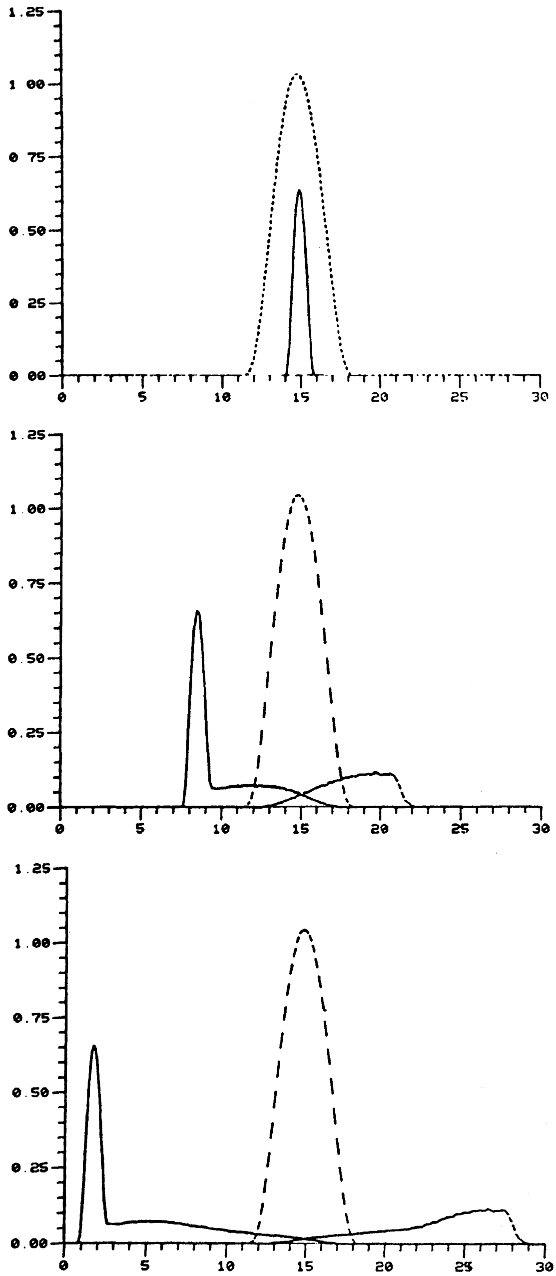


Figure 4. Explosive case when $A_2 = 1.1974 < \pi/2$. Here the interaction is stable.

Thus when the middle envelope contains one (or more) soliton ($A_2 > \pi/2$), the explosive instability occurs.

What happens if $A_2 < \pi/2$? In Figure 4, we see the results when $A_2 = 1.1974 < \pi/2$. In this case, a well defined final state occurs where the envelopes do separate, and the solution is stable.

In addition to no solitons in the middle envelope, there is one more condition necessary for unique solutions to exist to the inverse scattering equations [5]. When $r = +q^*$, we have $|a|^2 = 1 + |b|^2$ [7], and thus we must have $|b/a| < 1$ for the $Q_1$ and $Q_3$ envelopes in (12). For square colliding initial profiles, as in Figure 5, one can show [8] that this will be satisfied only if

$$\tan A_2 \sinh A_3 < 1. \tag{24}$$

If $A_2 = 1.133$, then (24) requires $A_3 < .452$. In Figure 5, we have $A_2 = 1.133$ and $A_3 = .5445$, so that (24) is not satisfied. In Figure 5b; $A_2$ has increased to $1.637 > \pi/2$, and in Figure 5c, an explosive spike is clearly developing. In Figure 6, we repeat the above, but with $A_3 = .389$ so that (24) is satisfied. As seen in Figure 6b, complete separation is occurring. As a test of the area theorem for the final envelopes, from (12), (13), and (15), one obtains

$$\tanh A_{3f} = \tanh A_{30}/\cos A_{20}, \tag{25a}$$

$$\tan A_{2f} = \tan A_{20} \cosh A_{3f}, \tag{25b}$$

which gives $A_{2f} = 1.348$. This is to be compared to the value of 1.347 obtained from the computer simulation.

Thus, we can say that if the explosive instability is to be avoided, not only must the middle envelope contain no solitons ($A_2 < \pi/2$), but also the initial state must be such that $|b/a| < 1$ for the final envelopes of $Q_1$ and $Q_3$.

3. **Soliton Decay Case.** In this case, typically the middle envelope has the highest frequency and all waves are positive-energy waves. Thus we may take $(\gamma_1, \gamma_2, \gamma_3) = (-, +, -)$ which from (10) gives $r = -q^*$ for all three envelopes. Now, all envelopes may contain solitons and the general dynamics is as indicated in Figure 2. But, there are two situations of special interest.

First, take a large middle envelope and slightly perturb it, as in Figure 7a. Here $A_2 = 6.40$, so that $Q_2$ contains two solitons, and we have a small blip of $Q_1$ to perturb it. From Figure 2, we then expect the final states of $Q_1$ and $Q_3$ to contain 2 solitons each. Furthermore, by (12), since $Q_3$ is zero and $Q_1$ is very small initially, $(b/a)$ for real $\lambda$ of these two final envelopes must also be small, giving that these two final

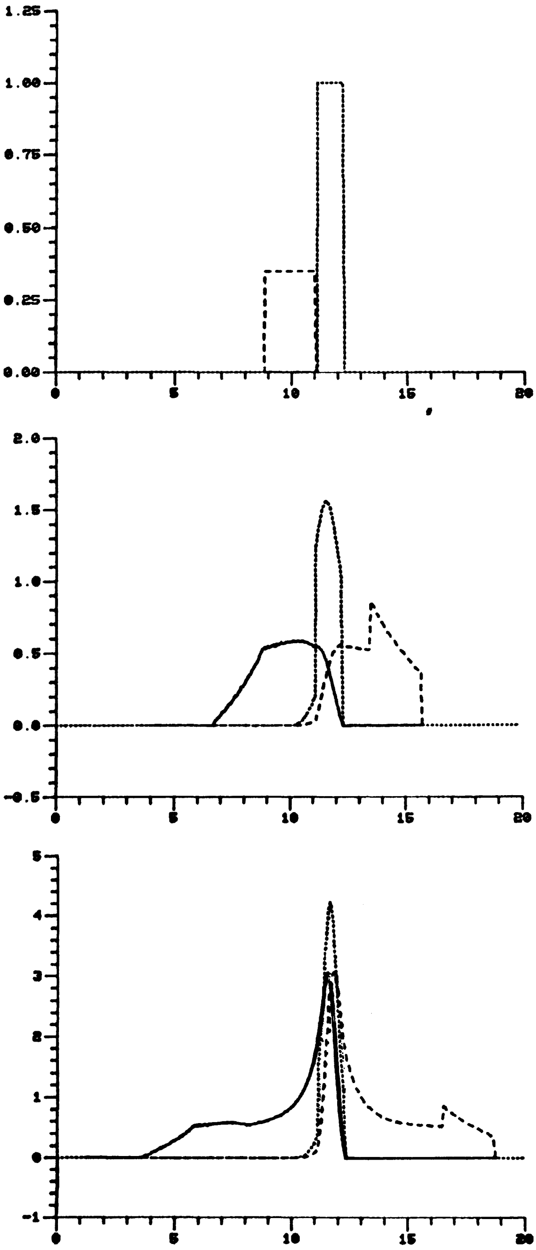


Figure 5. Explosive case for $Q_2$ and $Q_3$ colliding, with both envelopes large. Since $A_3 = .5445 > .452$ (see text), a singular spike again develops.

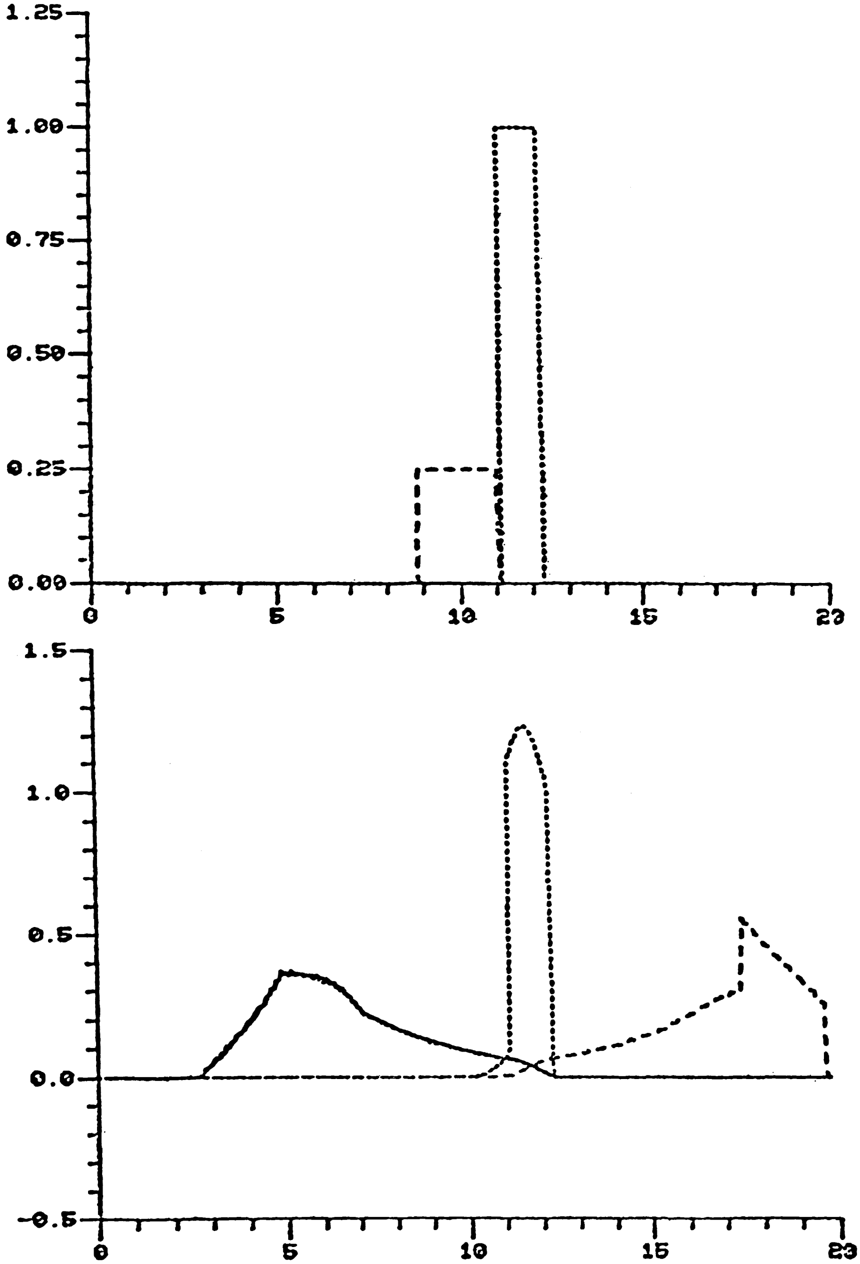


Figure 6. Explosive case for $Q_2$ and $Q_3$ colliding, where now $A_3 = .389 < .452$, and no singular spike develops.

envelopes must contain almost no radiation. Thus they will be almost pure 2-soliton solutions. In Figure 7b–e, we see the time development of this situation, and indeed, in Figure 7e, both $Q_1$ and $Q_3$ do have two peaks. In fact, from the initial conditions given in 7a, we can predict exactly what the parameters for these two-soliton should be, and we find excellent agreement between theory and simulations. Also, in Figure 8 we have the same situation where $A_2 = 3.25$ (one-soliton), and in Figure 9, we see what happens when $A_2 \simeq 16$ (five-solitons).

Of course, one should note the resulting simplicity when one describes what happens in terms of the nonlinear concepts. In Figures 7–9, the middle envelopes have decayed by emitting only solitons, and have retained their original radiation densities. In this "soliton decay case," the middle envelope is therefore (linearly) unstable whenever it initially contains one or more solitons.

The second situation corresponds to the "time-reversal" of Figure 2, whereby we have a collision between $Q_1$ and $Q_3$, producing $Q_2$. In Figure 10, we see the typical result when both $Q_1$ and $Q_3$ initially contains no solitons ($A_1 = 1.456$, $A_3 = 1.455 < \pi/2$). In Figure 10b, $Q_2$ is simply a nonlinear convolution of $Q_1$ and $Q_3$, with the simulation giving a final area of $A_2 = 1.4084$, and a final total radiation of $N_r^{(2)} = 2.5146$. The theory gives a final area of $A_2 = 1.4077$ and a final total radiation of $N_r^{(2)} = 2.5146$, both of which are in excellent agreement with the simulations. In Figure 11, we see what happens when $Q_1$ and $Q_3$ both contain one soliton each initially ($A_1 = 2.844$, $A_3 = 2.841 > \pi/2$). In Figure 11b, $Q_2$ has developed a very strong peak, and its area has gone to $A_2 = 3.011 > \pi/2$, showing that it now has one soliton. However, as we have already seen, this configuration is unstable, and later, $Q_2$ will decay and they will add one-soliton tails onto $Q_1$ and $Q_3$.

This process of $Q_2$ absorbing solitons from $Q_1$ and $Q_3$ is very sensitive to the pairing of the eigenvalues between $Q_1$ and $Q_3$. In the normal process whereby a soliton originally in $Q_2$ is given to both $Q_1$ and $Q_3$, the new solitons in $Q_1$ and $Q_3$ have equal eigenvalues (when $c_3 = -c_1$, $c_2 = 0$) of one half of the eigenvalue of the original soliton of $Q_2$. Conversely, to obtain the time-reversal of this, the eigenvalues of $Q_1$ and $Q_3$ must be equal. When a soliton in $Q_1$ has the same eigenvalue as a soliton in $Q_3$, we call these solitons "resonantly paired solitons," and the state achieved in Figure 11b only occurs for resonantly paired solitons. From this figure, we see that most of the original radiation density in $Q_1$ and $Q_3$ has been transmitted without any time delay. Of course, some of it was absorbed by $Q_2$, since $N_r^{(2)}$ is nonzero in Figure 11b, but this absorption of radiation density only occurs dur-

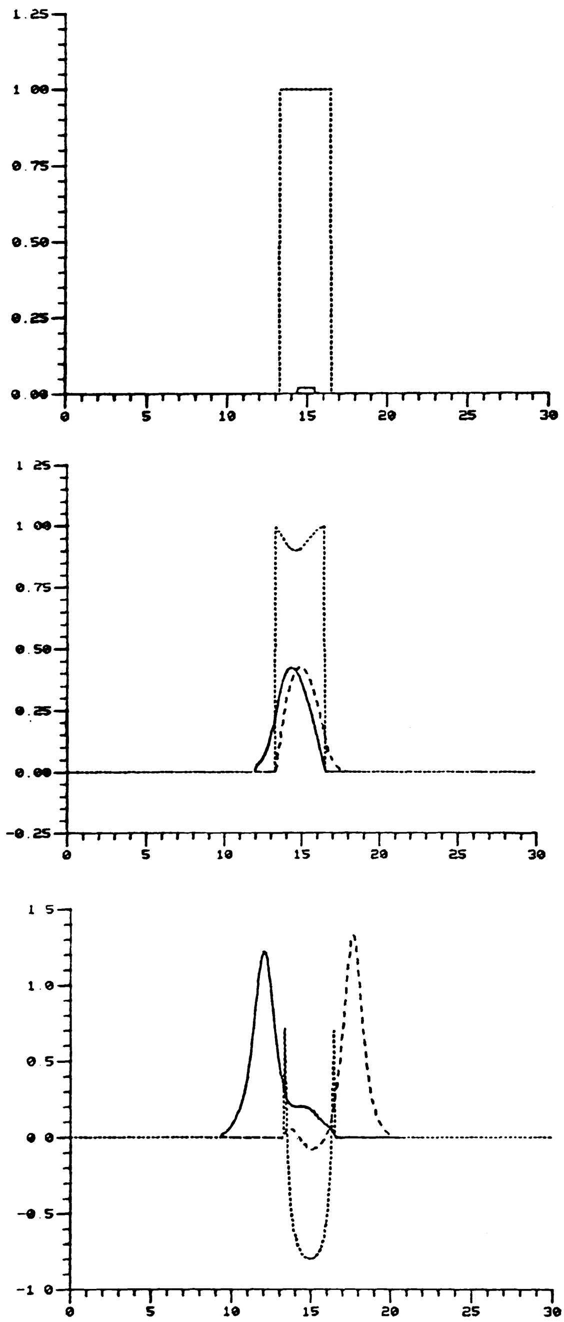
1.25
1.00
0.75
0.50
0.25
0.00
0
5
10
15
20
25
30
1.25
1.00
0.75
0.50
0.25
0.00
-0.25
1.5
1.0
0.5
0.0
-0.5
-1.0

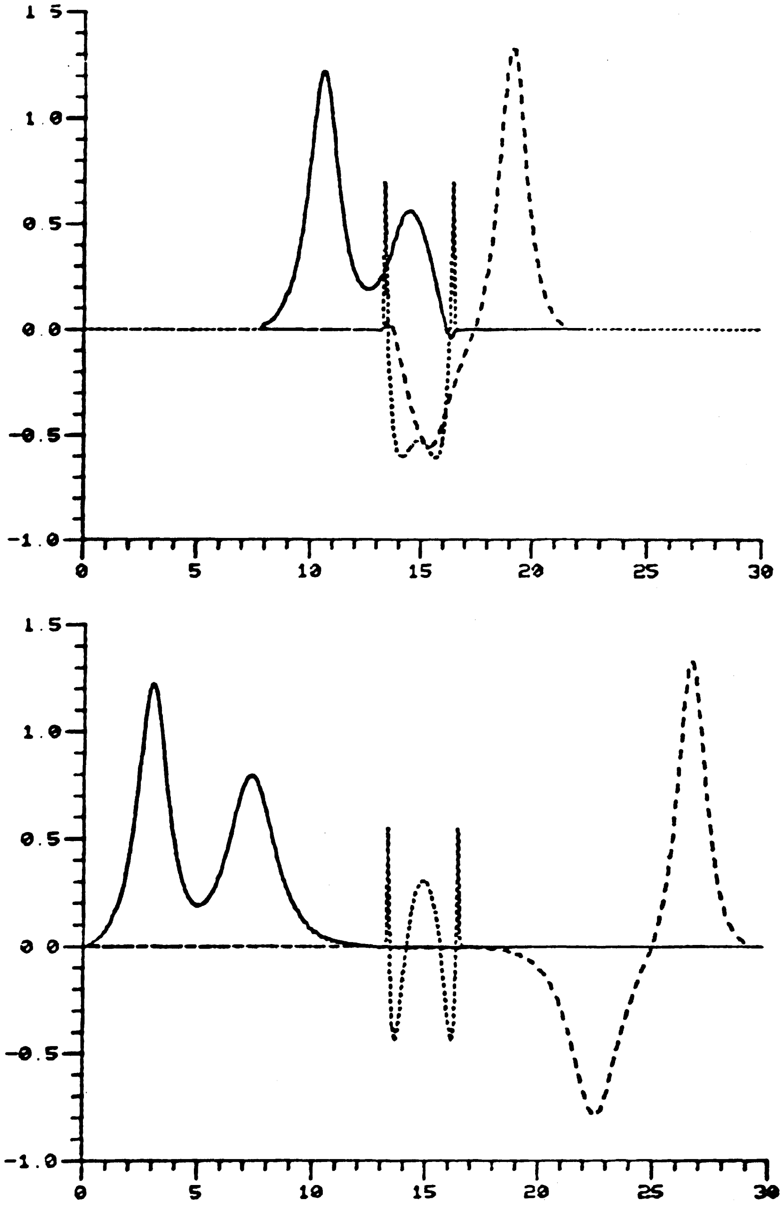


Figure 7. Soliton decay case for $A_2 = 6.40$, for which $Q_2$ initially contains two solitons. In Figure 7e, we see the final configuration where both $Q_1$ and $Q_3$ are two-soliton states and $Q_2$ has no solitons.

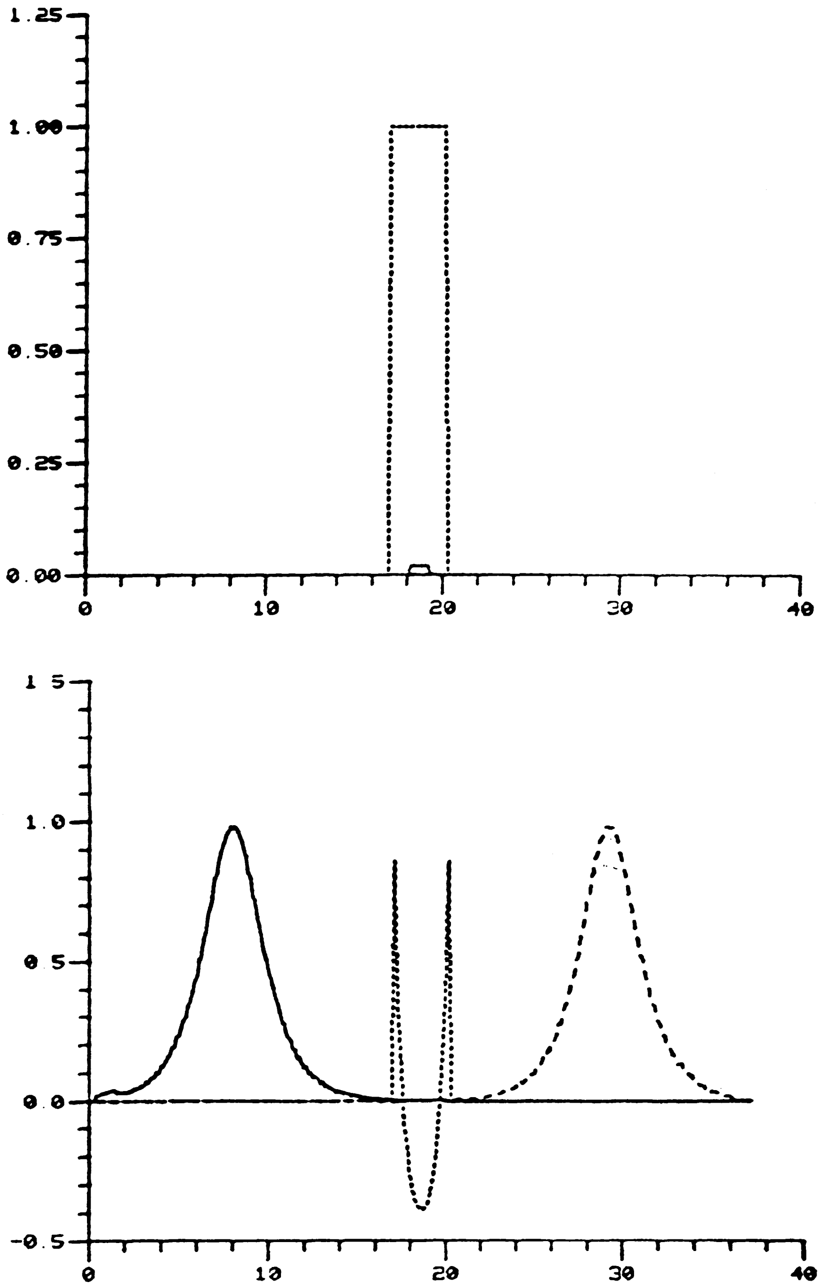


Figure 8. Soliton decay case for $A_2 = 3.25$, for which $Q_2$ only has one soliton initially.

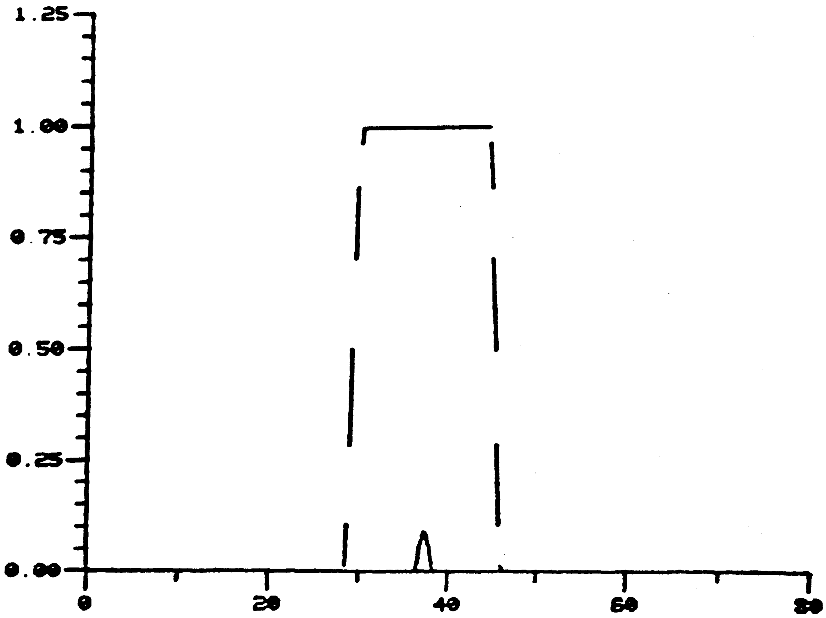


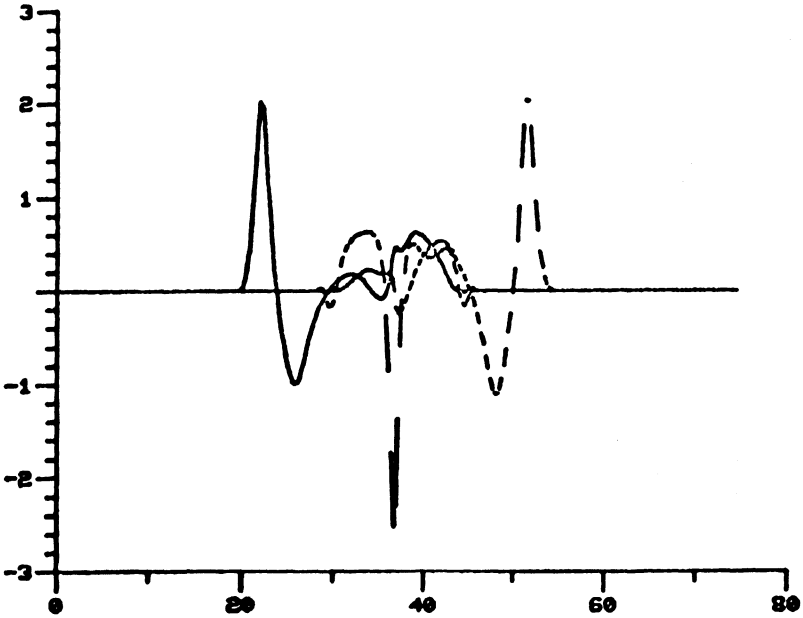


Figure 9 continued next page.

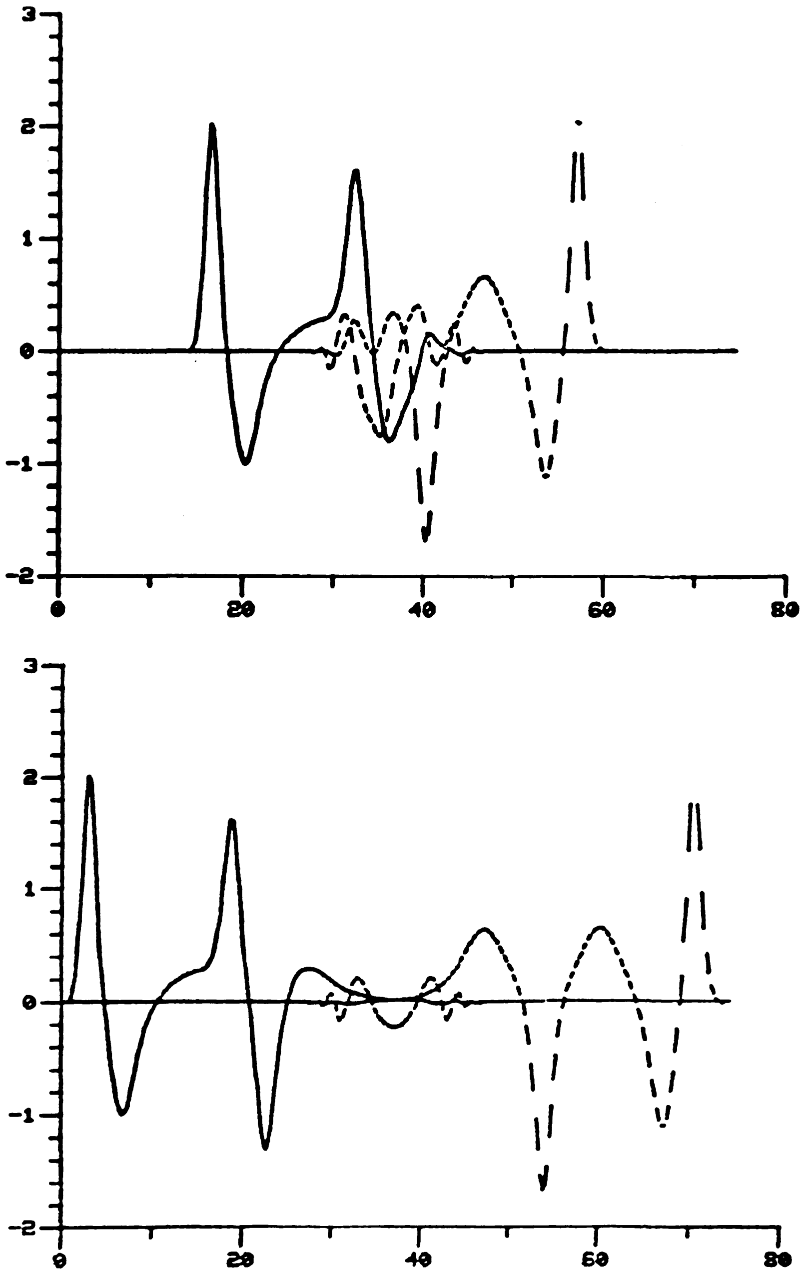


Figure 9. Soliton decay case for $A_2 \simeq 16$, for which $Q_2$ has five solitons initially.

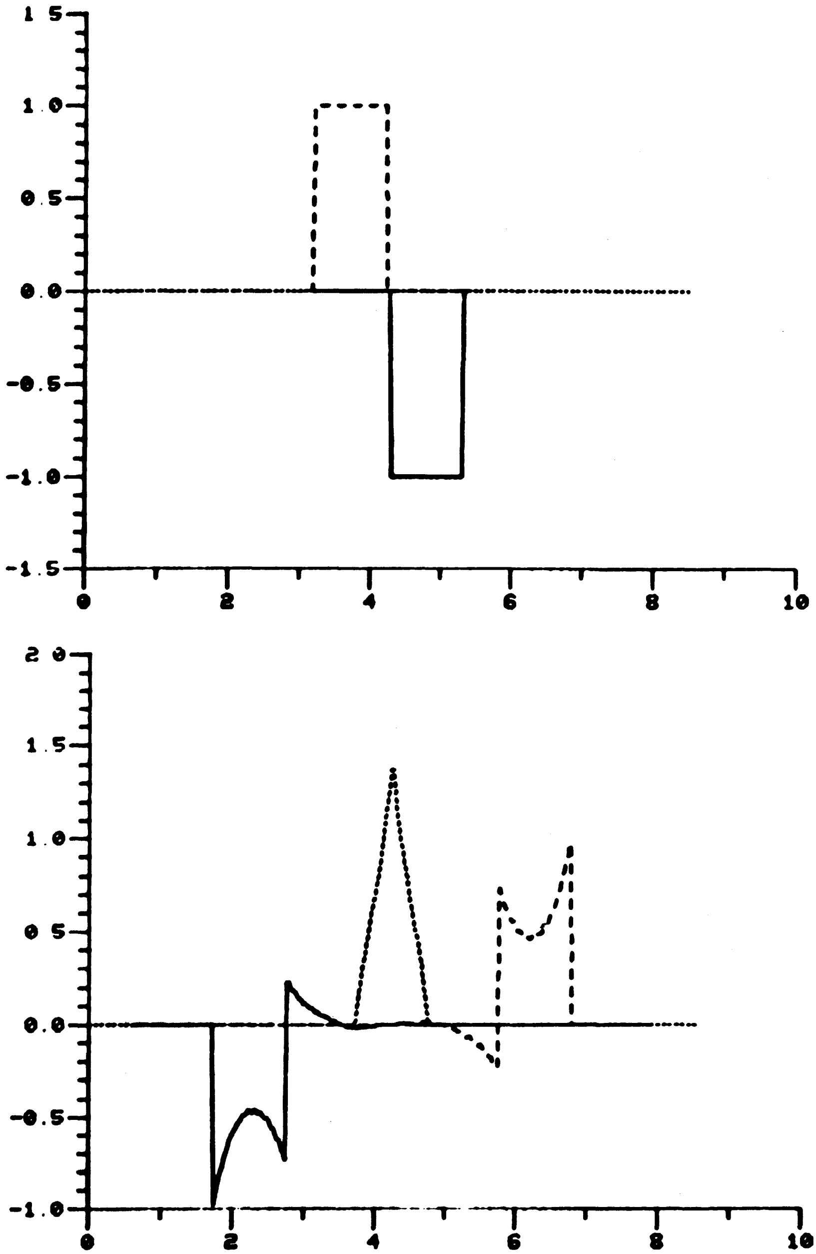


Figure 10. Soliton decay case for $Q_1$ and $Q_3$ colliding, where neither has any solitons initially.

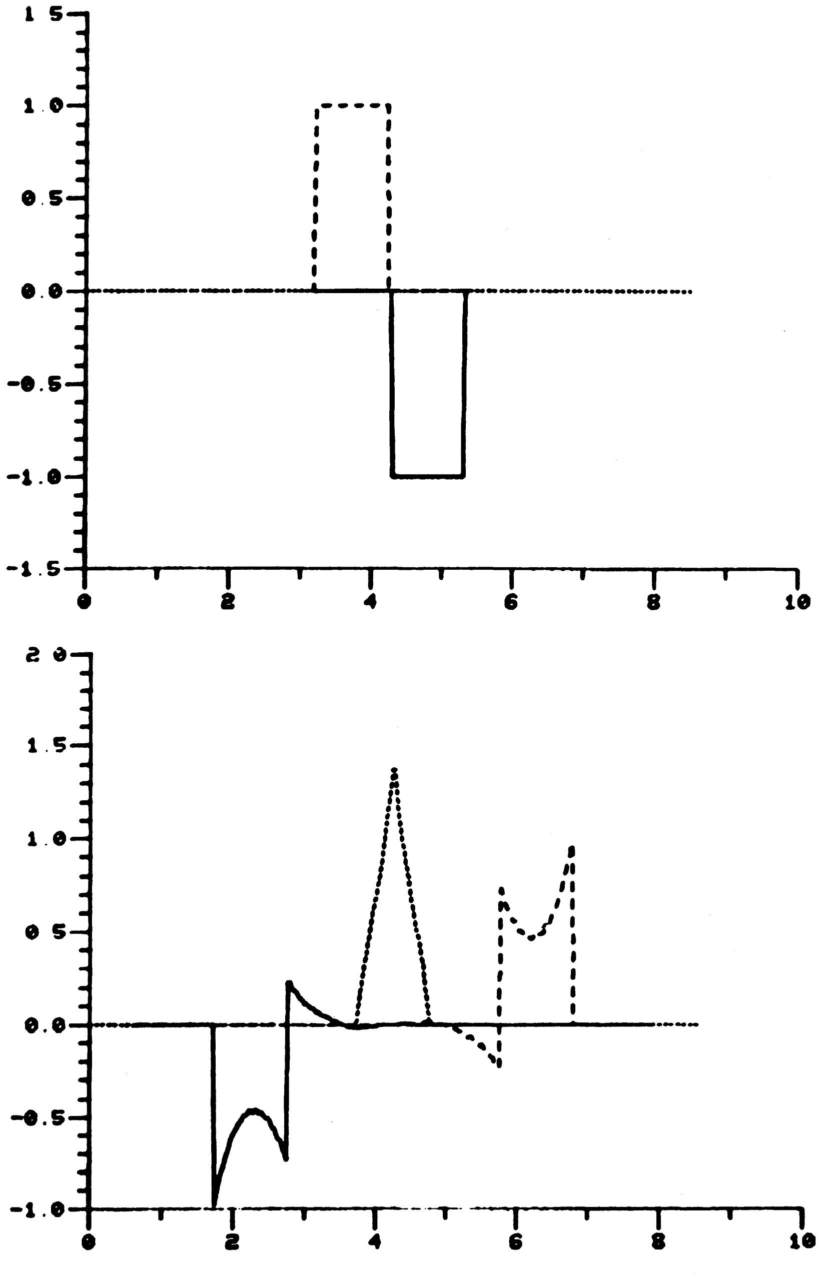


Figure 10. Soliton decay case for $Q_1$ and $Q_3$ colliding, where neither has any solitons initially.

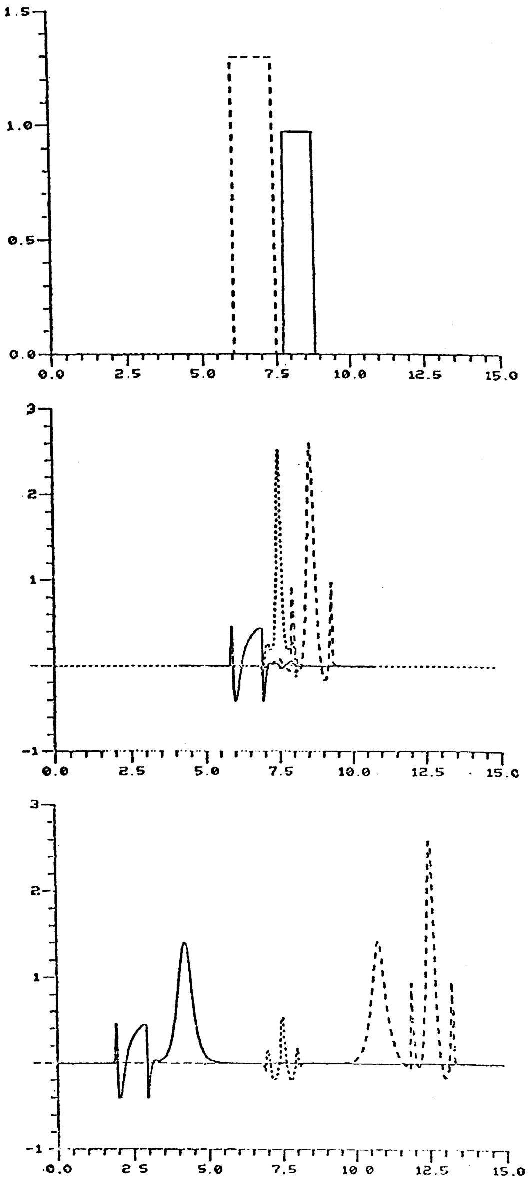


Figure 12. Soliton decay case for $Q_1$ and $Q_3$ colliding when $Q_1$ has two solitons, one of which is resonantly paired to the single soliton in $Q_3$. In Figure 12b, we see the intermediate state where $Q_2$ has spiked, and the unpaired soliton in $Q_3$ has been transmitted without any time delay. In Figure 12c, the middle envelope has decayed and added one-soliton tails onto $Q_1$ and $Q_3$.

ing the initial collision, since when $Q_2$ decays later, virtually no radiation is released.

Thus, during this collision, we know what happens to the radiation and the resonantly paired solitons. What happens to any unpaired solitons? To answer this, we look at the next simulation in Figure 12, where $Q_1$ has two solitons, the smallest eigenvalue of which is equal to the eigenvalue of the single soliton in $Q_3$. In Figure 12b, we see the intermediate state where $Q_2$ has absorbed the resonantly paired solitons (as well as some radiation density), with the remaining radiation density and the unpaired soliton (the central peak in $Q_1$) being transmitted without any time delay. Finally, in Figure 12c, we see the final state where $Q_2$ has decayed, releasing the two resonantly paired solitons, which form one-soliton tails onto $Q_1$ and $Q_3$.

In summary then, when $Q_1$ and $Q_3$ collide, $Q_2$ will initially absorb the required amount of radiation density from $Q_1$ and $Q_3$ as well as all resonantly paired solitons, with the remaining radiation density and unpaired solitons being transmitted without any time delay. Then later, $Q_2$ will decay, releasing the resonantly paired solitons, which then form $N$-soliton tails onto $Q_1$ and $Q_3$.

4. **The SBS Case.** The last case is called the SBS (stimulated backscattering) case, since typically, the highest frequency envelope is a laser pulse ($Q_3$), $Q_1$ is a backscattered laser envelope, and $Q_2$ is a positive energy plasma or acoustic wave of low velocity. Then we have $(\gamma_1, \gamma_2, \gamma_3) = (-, -, +)$ which gives

(25a) $$r^{(1)} = -q^{(1)*} \quad \text{(BS wave)},$$

(25b) $$r^{(2)} = +q^{(2)*} \quad \text{(Acoustic Wave)},$$

(25c) $$r^{(3)} = +q^{(3)*} \quad \text{(Incident Wave)}.$$

Now, since only the BS wave (which is usually zero initially) can have solitons, no soliton exchange effects will occur, and we shall only be interested in how the total radiation is exchanged.

Of prime importance in this case is the "reflection coefficient," $R$, which is the ratio of the backscattered total radiation (action) to the incident total radiation.

(26) $$R = \frac{N_f^{(1)}}{N_0^{(3)}} = \frac{\int_{-\infty}^{\infty} |q_f^{(1)}|^2 \, dx}{\int_{-\infty}^{\infty} |q_0^{(3)}|^2 \, dx},$$

where from (17)

(27) $$N_f^{(1)} = \frac{1}{\pi} \int_{-\infty}^{\infty} d\lambda \ln[1 + \Gamma_f^{(1)}(\lambda)],$$

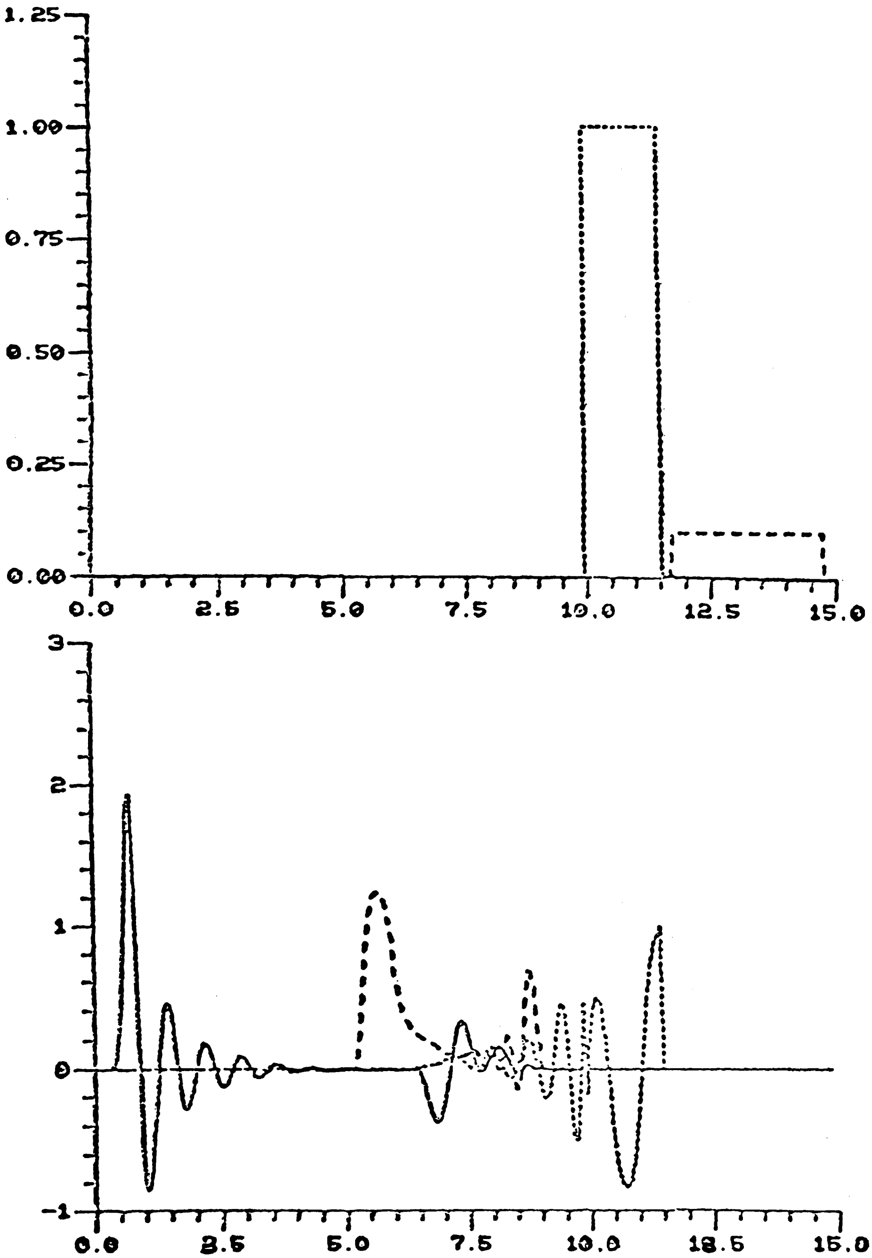


Figure 13. A typical example of the SBS case for a colliding laser and acoustic pulse. The backscattered pulse is the solid curve in Figure 13b.

and from (10) and (18)

$$\Gamma_f^{(1)} = \frac{\Gamma_0^{(2)}\Gamma_0^{(3)}}{1 + \Gamma_0^{(2)}} \,. \tag{28}$$

In Figure 13, we show the computer simulations for a typical nonlinear example. In Figure 13a, we see the initial profile, and in Figure 13b, we see essentially the final state. Note the characteristic large initial BS peak ($Q_1$) and the "ringing" which follows. In general (since only radiation is involved), this case is characterized by strong oscillations.

Directly from the simulations, we find that $R = .5874$ for this example. If we calculate $R$ from the theory, Eqs. (26)–(28), we find that

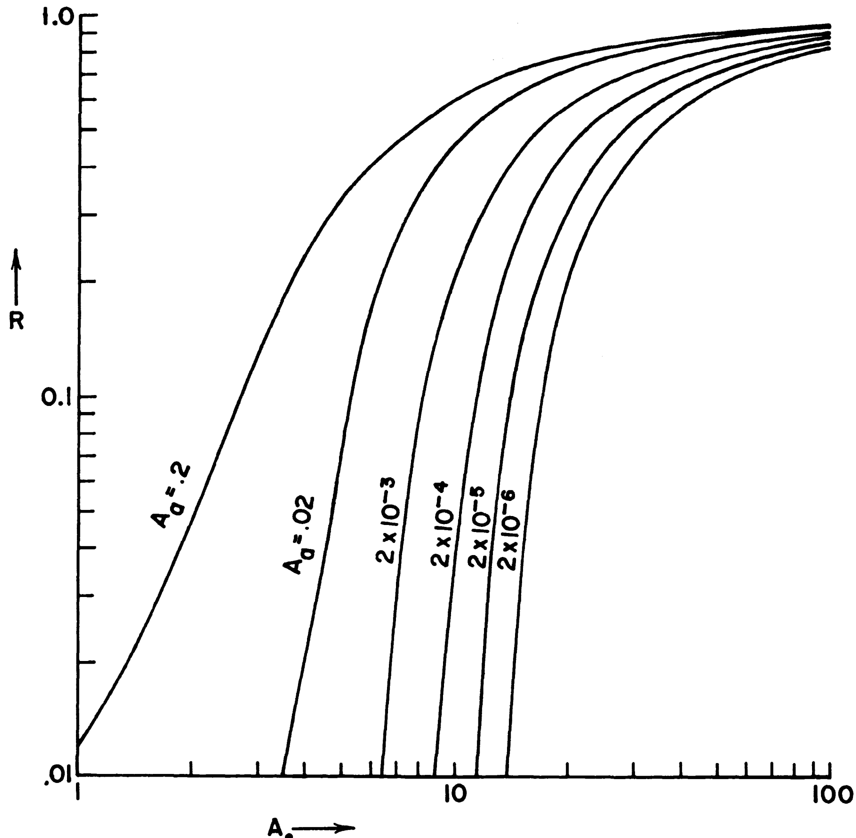


Figure 14. The SBS reflection coefficient, $R$, as a function of laser area ($A_\ell$) and amplitude ($Q_\ell$), for a fixed acoustic pulse.

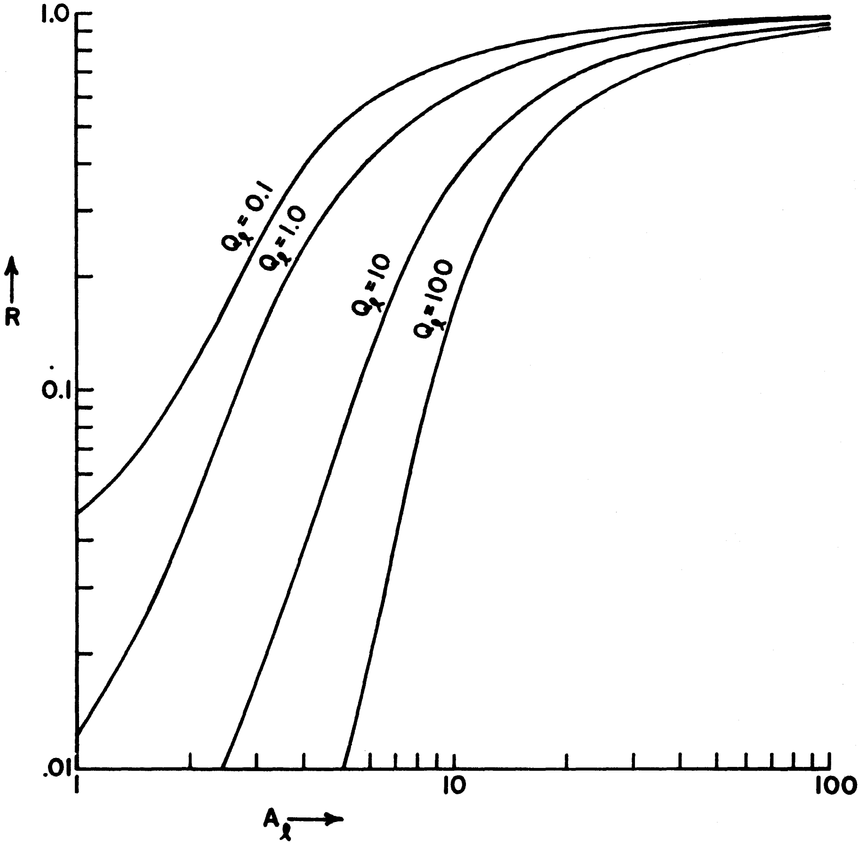


Figure 15. The SBS reflection coefficient, $R$, as a function of laser area ($A_\ell$) and acoustic area ($A_a$). Note the sharp threshold for $A_a$ small.

$R = .5445$. The discrepancy is entirely due to the strong BS oscillations still in the interaction region, which are very slowly decaying away.

In the final two figures, we show how $R$ is affected by the intial laser and acoustic pulses. If the initial envelopes are square, as in Figure 13, one has closed form solutions for $\Gamma_0^{(3)}$ and $\Gamma_0^{(2)}$, with which the integral in (27) may be numerically evaluated. In Figure 14 we show $R$ vs. the area of the laser pulse, $A_\ell$, for various laser amplitudes, $Q_\ell$, when the acoustical pulse has an amplitude of 0.1 and a length of 2.0. Note that although $R \to 1$ for sufficiently large $A_\ell$, if we compress the laser pulse ($A_\ell$ fixed and increase $Q_\ell$), $R$ decreases. In Figure 15, we again plot $R$ vs. $A_\ell$, but now for various values of the area of the acoustic pulse, $A_a$, with the amplitudes of the laser (acoustic) pulse fixed at

1.0 (0.1). One notes that as $A_a$ decreases, we are seeing a "threshold" appear. Returning to (26–28), one can show [8] that this threshold area of the laser pulse is given by

$$A_\ell \simeq \sinh^{-1}(1/A_a). \tag{29}$$

When the area of the laser pulse is less than the above value, $R \simeq 0$, and when $A_\ell$ rises above the above value, $R$ rapidly rises up to an order of unity.

## References

1. D. J. Kaup, *Applications of the inverse scattering transform* I: *Self-induced transparency*, these Proceedings.

2. The computer simulations shown here were supplied through the courtesy of Professor A. Bers and A. Rieman of MIT.

3. V. E. Zakharov and S. V. Manakov, *Resonant interaction of wave packets in nonlinear media,* Sov. Phys.-JETP Lett. **18**, (1973), 243–245.

4. ———, *On the theory of resonant interaction of wave packets in nonlinear media,* Jetp **69** (1975), 1654–1673.

5. D. J. Kaup, *The three-wave interaction—a nondispersive phenomenon,* Stud. Appl. Math. **55** (1976), 9–44.

6. V. E. Zakharov and A. B. Shabat, *Exact theory of two-dimensional self-focusing and one-dimensional self-modulation of waves in nonlinear media,* Sov. Phys.-JETP **34** (1972), 62–69.

7. M. J. Ablowitz, D. J. Kaup, A. C. Newell, and H. Segur, *The inverse scattering transform—Fourier analysis for nonlinear problems,* Stud. Appl. Math. **53** (1974), 249–315.

8. D. J. Kaup, A. Bers, and A. Rieman (in preparation).

9. D. J. Kaup, *Exact quantization of the nonlinear Schrödinger equation.* J. Math. Phys. **16** (1975) 2036–2041.

Department of Physics, Clarkson College of Technology,
Potsdam, NY 13676